LETTER

doi:10.1038/nature13582

# Stochasticity of metabolism and growth at the single-cell level

Daniel J. Kiviet[1,2,3]*, Philippe Nghe[1]†*, Noreen Walker[1], Sarah Boulineau[1], Vanda Sunderlikova[1] & Sander J. Tans[1]

**Elucidating the role of molecular stochasticity[1] in cellular growth is central to understanding phenotypic heterogeneity[2] and the stability of cellular proliferation[3]. The inherent stochasticity of metabolic reaction events[4] should have negligible effect, because of averaging over the many reaction events contributing to growth. Indeed, metabolism and growth are often considered to be constant for fixed conditions[5,6]. Stochastic fluctuations in the expression level[1,7–9] of metabolic enzymes could produce variations in the reactions they catalyse. However, whether such molecular fluctuations can affect growth is unclear, given the various stabilizing regulatory mechanisms[10–12], the slow adjustment of key cellular components such as ribosomes[13,14], and the secretion[15] and buffering[16,17] of excess metabolites. Here we use time-lapse microscopy to measure fluctuations in the instantaneous growth rate of single cells of *Escherichia coli*, and quantify time-resolved cross-correlations with the expression of *lac* genes and enzymes in central metabolism. We show that expression fluctuations of catabolically active enzymes can propagate and cause growth fluctuations, with transmission depending on the limitation of the enzyme to growth. Conversely, growth fluctuations propagate back to perturb expression. Accordingly, enzymes were found to transmit noise to other unrelated genes via growth. Homeostasis is promoted by a noise-cancelling mechanism that exploits fluctuations in the dilution of proteins by cell-volume expansion. The results indicate that molecular noise is propagated not only by regulatory proteins[18,19] but also by metabolic reactions. They also suggest that cellular metabolism is inherently stochastic, and a generic source of phenotypic heterogeneity.**

To investigate the dynamics of cellular growth, we followed individual *E. coli* cells growing on different nutrients. Among them was the synthetic sugar lactulose[20], which is imported and catabolized by the LacY and LacZ enzymes like its analogue lactose, but unlike lactose does not induce *lac* operon expression (Fig. 1a). Mixtures of lactulose and the gratuitous inducer isopropyl-β-D-thiogalactoside (IPTG) thus allowed us to vary the mean *lac* expression level independently and hence to explore different regimes of noise transmission. We determined the instantaneous growth rate $\mu(t)$ of individual cells within microcolonies at sub-cell-cycle resolution for various growth conditions, using time-lapse microscopy[19] at high acquisition rates and automated image analysis (Supplementary Information). We found that $\mu(t)$ varied considerably in time, both within one cell-cycle and between different cell-cycles (Fig. 1b, c and Extended Data Fig. 1), with noise intensities (standard deviation over the mean) ranging between 0.2 and 0.4 (Fig. 1d). Consistently,

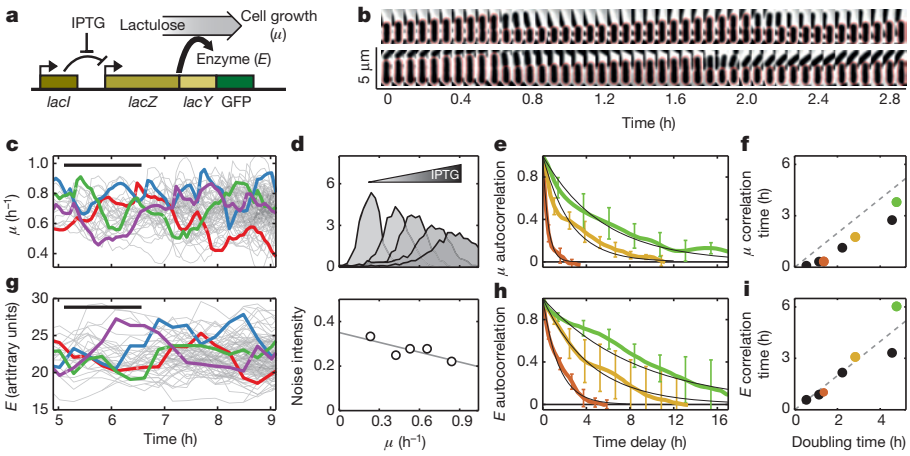


**Figure 1 | Growth rate variability in single *E. coli* cells.** **a**, Schematic diagram of the studied system. Lactulose is metabolized by the *lac* enzymes, but does not induce *lac* expression. Mean *lac* expression can hence be varied independently by the inducer IPTG. GFP is fused transcriptionally in the *lac* operon (Extended Data Table 2). **b**, Aligned phase-contrast images for two lineages. Microcolonies were grown on polyacryl pads (0.1% lactulose and 200 μM IPTG) for eight to nine generations. Up to 48 images were taken per hour. Red line: cell boundary from image analysis. **c**, Instantaneous growth rate $\mu(t)$ against time, determined by fitting exponentials to the cellular length. Four lineages are coloured for clarity. Black bar, mean division time; light points, division events. **d**, Top: histograms of $\mu$ values for different IPTG levels. Bottom: noise intensity (standard deviation over the mean). **e**, Autocorrelation function of $\mu(t)$ for low (4 μM, green), intermediate (6 μM, ochre) and high (200 μM, brown) IPTG levels. For clarity, error bars denoting the standard deviation are indicated only for a fraction of the points. Black lines: exponential fits that provide the correlation time. Correlation functions were determined along the branched lineages (Extended Data Fig. 8). **f**, Graph of $\mu(t)$ correlation time versus mean doubling time. Colours are as in **e**; black points are for growth on defined rich, lactose, succinate and acetate (in order of increasing doubling time). **g**–**i**, As **c**, **e** and **f**, but for the fluorescence intensity reporting for $E(t)$ within single cells. Protein concentrations were determined by the mean fluorescence per unit area (Extended Data Fig. 1e–g).

[1]FOM institute AMOLF, Science Park 104, 1098 XG Amsterdam, the Netherlands. [2]Department of Environmental Systems Science, ETH Zurich, Universitaetsstrasse 16, 8092 Zurich, Switzerland. [3]Department of Environmental Microbiology, Eawag, Ueberlandstrasse 133, 8600 Duebendorf, Switzerland. †Present address: Laboratoire de Biochimie, UMR 8231 CNRS/ESPCI, École Supérieure de Physique et de Chimie industrielles, 10 rue Vauquelin, 75005 Paris, France.
*These authors contributed equally to this work.

the growth rates of sister cells were significantly correlated (Extended Data Fig. 2). We found that the typical timescales of the fluctuations were somewhat smaller than the mean cellular doubling time, as quantified by the autocorrelation functions $R_{\mu\mu}(\tau)$ (Fig. 1e, f). Such a scaling with doubling time is typical for protein concentration fluctuations[21]. Thus, the data indicated randomly fluctuating growth limitations, and suggested they could be caused by concentration fluctuations of cellular components.

To study the relation between growth and *lac* enzymes, we quantified the fluctuations in the *lac* production rate $p(t)$ and concentration $E(t)$ using green fluorescent protein (GFP) labelling (Fig. 1a, g–i and Extended Data Fig. 1). We computed the cross-correlation functions $R_{p\mu}(\tau)$ and $R_{E\mu}(\tau)$, which indicate whether expression fluctuations correlate with $\mu$-fluctuations occurring time $\tau$ later, and thus inform on the direction of transmission[9,22]. Both $R_{p\mu}(\tau)$ and $R_{E\mu}(\tau)$ showed positive correlations regardless of the IPTG concentration (Fig. 2a, e–g). Their shapes and symmetries did depend on IPTG, however. At low and intermediate IPTG, $R_{E\mu}(\tau)$ was nearly symmetric around $\tau = 0$ while $R_{p\mu}(\tau)$ was asymmetric with larger weight at $\tau > 0$ (Fig. 2e, f and Extended Data Fig. 3). This would indicate that $p$ fluctuations on average correlated more strongly with $\mu$ fluctuations that occur later. Such a delay in $\mu$ is consistent with the idea that *lac* expression fluctuations produce variations in lactulose catabolism, which in turn propagate through the metabolic network and perturb growth.

High IPTG $R_{E\mu}(\tau)$ displayed a positive peak at $\tau < 0$ (Fig. 2g and Extended Data Fig. 3). Thus, $E$ fluctuations correlated more strongly with $\mu$ fluctuations occurring earlier, which suggested backward transmission from growth to expression. Such a growth-to-expression coupling could be caused by specific regulatory interactions[13,23,24], or more generally by growth fluctuations that cause variations in general components that are required for transcription and translation. Overall, the data suggested that noise not only propagated forward, from expression to growth, but also backward, from growth to expression.

To determine whether back-and-forth transmission could explain the correlations, we developed a stochastic model. A black-box approach was followed, in which noise propagation is represented by phenomenological transmission coefficients that do not specify molecular details (Fig. 2b). Despite the circulating noise, the system could be decomposed into distinct noise transmission modes; here termed the *lac* catabolism, common noise and dilution modes (Fig. 2d). The cross-correlation curves for all induction levels (Fig. 2e–g) were fitted jointly, using the transmission strength from the common noise source to $p$ as a single free parameter (Fig. 2h–j).

The effects of induction could be explained by altered intensities of the modes. At low and intermediate IPTG, the *lac* catabolism mode was dominant, with *lac* noise causing up to 30% of the growth noise (Extended Data Table 1). At higher IPTG this mode weakened because of decreased transmission from $E$ to $\mu$. This decrease is plausible, as catalysed reactions are less dependent on catalyst when the latter is abundant, consistent with the observed relation between the mean $\bar{E}$ and $\bar{\mu}$ (Fig. 2c). On the other hand, the rather constant $R_{p\mu}(0)$ (Fig. 2e–g) indicated that the common-noise mode had an almost fixed intensity for all IPTG concentrations. To probe the generality of this mode further, we made a number of genetic modifications. We found that it remained active when we knocked-out the *lac* repressor, changed the GFP position within the operon, altered the type of fluorescent protein or used an exogenous constitutive promoter (Extended Data Fig. 4a–d). These data suggest that common noise transmits to expression in general, which does not exclude additional coupling by specific regulatory interactions.

Next, we tested key findings. First, if the asymmetry in $R_{p\mu}(\tau)$ (Fig. 2e, f) is indeed caused by *lac* catabolism, this asymmetry should be suppressed when carbon enters central metabolism via another pathway. Growth on acetate was similarly slow as on lactulose and low induction, but $R_{p\mu}(\tau)$ was now indeed nearly symmetric (Fig. 3a, b and Extended Data Fig. 3). At the same time, $R_{E\mu}(\tau)$ became more asymmetric as predicted for a dominant common noise mode transmission (Fig. 3a, b and Extended Data Fig. 3). When growing on other natural substrates including lactose, the $R_{E\mu}$ peak-width scaled roughly with doubling time consistent with dilution setting the transmission delay timescales (Fig. 3b and Extended Data Fig. 5). To test further whether *lac* fluctuations could be

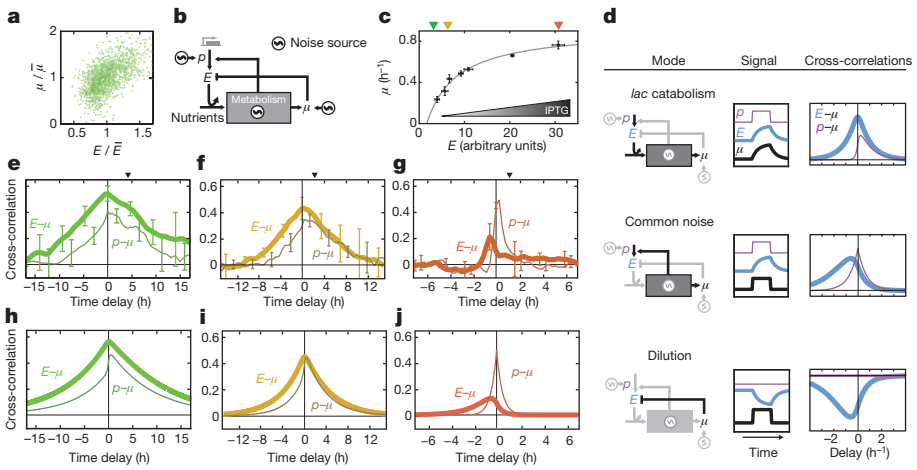


**Figure 2 | Cross–correlation functions and mathematical model.** **a**, Instantaneous growth rate against *lac* enzyme concentration from one microcolony, corresponding to the cross-correlation value $R_{E\mu}(0)$ in **e**. **b**, Model of the coupling between expression and growth noise. Two noise sources are specific to $p$ and $\mu$, one is common to $p$ and $\mu$. Correlations arise when noise emitted from one source is received by two observables ($p$, $E$ or $\mu$). Analytical solutions revealed all contributing pathways, and showed they were finite despite the looped network structure (Supplementary Information). **c**, The mean growth rate versus the mean expression level, as measured for different levels of IPTG induction. Line: fit to a Monod growth model. **d**, Three classes of noise transmission modes. As an example, a noise source (left) emits a block wave, giving rise to signals $\mu$, $p$ and $E$ (middle) and their cross-correlations (right). Other pathways contribute as well. For instance, common noise can also drive the catabolism mode. **e**–**g**, Cross-correlation functions $R_{p\mu}(\tau)$ for the enzyme production rate $p(t)$ and growth rate $\mu(t)$ (thin line), as well as $R_{E\mu}(\tau)$ for the enzyme concentration $E(t)$ and $\mu(t)$ (thick line). Growth is on lactulose (0.1%) with IPTG: 4 μM (**e**), 6 μM (**f**), 200 μM (**g**). Top triangles indicate mean division time. Error bars denoting the standard deviation are indicated for some data points only. The main features were robust to changing the growth determination method and taking the cell width into account (Extended Data Fig. 4e–h). Growth and expression differences typically did not correlate with location within the microcolony (Extended Data Fig. 4i). Protein production rates were determined by the time-derivative of the total fluorescence per cell (Extended Data Fig. 1e–h). **h**–**j**, Fits to the experimental data (**e**–**f**).

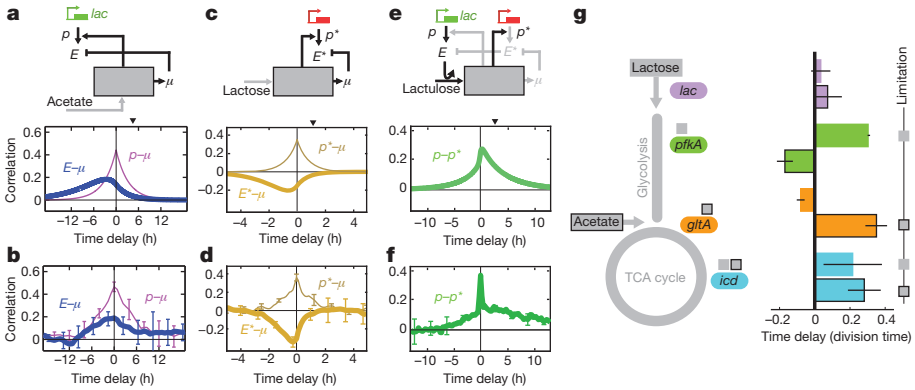


**Figure 3 | Model predictions and experimental tests.** Top: re-wired noise transmission networks with predicted dominant pathways (black). Coloured genes indicate labelling with GFP and mCherry. Middle: predicted cross-correlation with mean doubling time (triangle). Bottom: measured cross-correlation. Error bars denote the standard deviation. **a**, **b**, For growth on acetate the *lac* enzymes are catabolically inactive. **c**, **d**, Gene with a weaker coupling from common noise to expression (compared with the *lac* operon), leading to dominant dilution. **e**, **f**, Transmission from the *lac* genes to another gene via growth. When the *lac* genes do not transmit because cells grow on acetate, the correlation is symmetric (Extended Data Fig. 7c, d). **g**, Time delays for *lac*, *pfkA*, *gltA* and *icd* in lactose (not boxed) and acetate media (boxed), as derived from the correlation functions $R_{p\mu}(\tau)$ (Extended Data Fig. 7e). Small square boxes indicate which gene is considered limiting in steady-state in a particular medium (see main text).

causal in the growth noise, we exposed the cells to IPTG pulses in a microfluidic device. The resulting pulses in *lac* expression were indeed followed by a pulse in growth (Extended Data Fig. 6a). Next, we aimed to mimic common noise fluctuations by growing cells on glucose minimal medium and pulsing with amino acids. These pulses indeed produced transient increases in $\mu$ and $p$ (Extended Data Fig. 6b), consistent with common noise propagating to enzyme expression and to growth.

Second, the network structure implied a homeostatic control mechanism: upward fluctuations in common noise increase $E$ when transmitted via $p$, but also decrease $E$ when transmitted via $\mu$ (Fig. 2b). These opposing effects offer a direct prediction: if the positive pathway dominates, $R_{E\mu}(\tau)$ should be positive, as is the case so far. If the negative pathway would dominate, however, $R_{E\mu}(\tau)$ should become negative (Fig. 3c). One cannot manipulate how volume changes affect dilution. To tilt the balance, we thus looked for constructs with a weaker coupling to common noise in the positive pathway, as measured by $R_{p\mu}(0)$. A constitutively expressed mCherry with a twofold lower $R_{p^*\mu}(0)$ indeed displayed negative $R_{E^*\mu}(\tau)$ (Fig. 3d and Extended Data Fig. 3). Thus, two parallel antagonistic pathways that together form a so-called incoherent feed-forward network motif[25] can partly cancel noise. This cancelling also explains why $R_{E\mu}(0)$ is low even though $R_{p\mu}(0)$ is high at high induction where common noise dominates (Fig. 2g). Interestingly, while up-fluctuations in $\mu$ are associated with up-fluctuations in $E$ (Fig. 2g), increases in mean $\bar{\mu}$ lead to decreases in $\bar{E}$ (Extended Data Fig. 5e)[13,23]. These opposing dependencies suggest that different mechanisms underlie these two types of expression variation.

Third, if *lac* enzymes transmit to growth and growth transmits to expression in general, then *lac* enzymes ought to transmit also to other genes. Hence we quantified $p^*(t)$ of mCherry controlled by promoters with no known functional interactions with the *lac* system. For lactulose and low induction, mCherry fluctuations indeed occurred after *lac* fluctuations on average (Fig. 3f and Extended Data Fig. 7a, b) in accordance with predictions (Fig. 3e). In contrast, this delay was absent for acetate, which is consistent because *lac* then does not transmit to growth (Extended Data Fig. 7c, d). Noise in *lac* expression can thus couple to other genes without specific regulatory interactions.

For the *lac* genes, the *lac* catabolism mode transmitted to growth only when the mean *lac* expression was kept artificially low and limited the mean growth rate. Hence, we wondered whether limiting enzymes in central metabolism could similarly perturb growth. For growth on lactose, glycolysis is considered limited by *pfkA*, and the tricarboxylic acid cycle by *icd* but not by *gltA*; while in acetate, *gltA* is limiting, *icd* may be limiting but *pfkA* is not[26–28]. We indeed observed positive time delays in $R_{p\mu}$ for *pfkA* and *icd* in lactose, and for *gltA* and *icd* in acetate, but not in the other cases (Fig. 3g and Extended Data Fig. 7e). This pattern of correlation delays is consistent with the mechanism found for *lac*, in which growth limitation in steady-state resulted in noise transmission to growth. Notably, the differences in noise transmission behaviour were observed for enzymes catalysing nearby reactions in the pathway. For instance, *icd* acts almost directly after *gltA*, but *icd* displayed delayed correlation in lactose while *gltA* did not. This excludes the possibility that the delayed correlations are caused by synchronous fluctuations of *pfkA*, *gltA*, *icd* and other central metabolic genes. Together, the results indicate that expression-to-growth noise propagation occurs more generally for limiting genes.

Our study shows that fluctuations in gene expression can affect the growth stability of a cell, and, in turn, growth noise affects gene expression. This entanglement between growth and expression noise reflects the inherent auto-catalytic nature of self-replicating systems: metabolic enzymes help synthesize the building blocks for their own synthesis. The results raise the question how different fluctuating metabolic activities within the cell are coordinated, and which regulatory mechanisms are implicated in maintaining growth homeostasis. Metabolic stochasticity could allow clonal cells in a population to adopt a wide spectrum of metabolic states, and hence enable bet-hedging strategies to exploit new conditions optimally. Metabolic stochasticity could represent a generic source of cellular heterogeneity[29], but also prevent optimal growth[30] and limit efficient biosynthesis. Novel approaches are required to incorporate noise transmission within the current theoretical framework of metabolism.

**Online Content** Methods, along with any additional Extended Data display items and Source Data, are available in the online version of the paper; references unique to these sections appear only in the online paper.

**Received 8 February 2013; accepted 16 June 2014.**
**Published online 3 September 2014.**

1. Wilkinson, D. J. Stochastic modelling for quantitative description of heterogeneous biological systems. *Nature Rev. Genet.* **10,** 122–133 (2009).
2. Eldar, A. & Elowitz, M. B. Functional roles for noise in genetic circuits. *Nature* **467,** 167–173 (2010).
3. Heiden, M. G. V., Cantley, L. C. & Thompson, C. B. Understanding the Warburg effect: the metabolic requirements of cell proliferation. *Science* **324,** 1029–1033 (2009).
4. Lu, H. P., Xun, L. Y. & Xie, X. S. Single-molecule enzymatic dynamics. *Science* **282,** 1877–1882 (1998).
5. Fell, D. *Understanding the Control of Metabolism* (Portland, 1997).
6. Herrgard, M. J., Covert, M. W. & Palsson, B. O. Reconstruction of microbial transcriptional regulatory networks. *Curr. Opin. Biotechnol.* **15,** 70–77 (2004).
7. Elowitz, M. B., Levine, A. J., Siggia, E. D. & Swain, P. S. Stochastic gene expression in a single cell. *Science* **297,** 1183–1186 (2002).

8. Ferguson, M. L. *et al.* Reconciling molecular regulatory mechanisms with noise patterns of bacterial metabolic promoters in induced and repressed states. *Proc. Natl Acad. Sci. USA* **109,** 155–160 (2012).
9. Munsky, B., Neuert, G. & van Oudenaarden, A. Using gene expression noise to understand gene regulation. *Science* **336,** 183–187 (2012).
10. Neidhardt, F. C., Ingraham, J. L. & Schaechter, M. *Physiology of the Bacterial Cell: A Molecular Approach* (Sinauer, 1990).
11. Rodriguez, M., Good, T. A., Wales, M. E., Hua, J. P. & Wild, J. R. Modeling allosteric regulation of de novo pyrimidine biosynthesis in *Escherichia coli*. *J. Theor. Biol.* **234,** 299–310 (2005).
12. Hart, Y. *et al.* Robust control of nitrogen assimilation by a bifunctional enzyme in *E. coli*. *Mol. Cell* **41,** 117–127 (2011).
13. Klumpp, S., Zhang, Z. & Hwa, T. Growth rate-dependent global effects on gene expression in bacteria. *Cell* **139,** 1366–1375 (2009).
14. Yun, H. S., Hong, J. & Lim, H. C. Regulation of ribosome synthesis in *Escherichia coli*: effects of temperature and dilution rate changes. *Biotechnol. Bioeng.* **52,** 615–624 (1996).
15. el-Mansi, E. M. & Holms, W. H. Control of carbon flux to acetate excretion during growth of *Escherichia coli* in batch and continuous cultures. *J. Gen. Microbiol.* **135,** 2875–2883 (1989).
16. Wilson, W. A. *et al.* Regulation of glycogen metabolism in yeast and bacteria. *FEMS Microbiol. Rev.* **34,** 952–985 (2010).
17. Levine, E. & Hwa, T. Stochastic fluctuations in metabolic pathways. *Proc. Natl Acad. Sci. USA* **104,** 9224–9229 (2007).
18. Pedraza, J. M. & van Oudenaarden, A. Noise propagation in gene networks. *Science* **307,** 1965–1969 (2005).
19. Rosenfeld, N., Young, J. W., Alon, U., Swain, P. S. & Elowitz, M. B. Gene regulation at the single-cell level. *Science* **307,** 1962–1965 (2005).
20. Dean, A. M. A molecular investigation of genotype by environment interactions. *Genetics* **139,** 19–33 (1995).
21. Austin, D. W. *et al.* Gene network shaping of inherent noise spectra. *Nature* **439,** 608–611 (2006).
22. Dunlop, M. J., Cox, R. S., III, Levine, J. H., Murray, R. M. & Elowitz, M. B. Regulatory activity revealed by dynamic correlations in gene expression noise. *Nature Genet.* **40,** 1493–1498 (2008).
23. Scott, M., Gunderson, C. W., Mateescu, E. M., Zhang, Z. & Hwa, T. Interdependence of cell growth and gene expression: origins and consequences. *Science* **330,** 1099–1102 (2010).
24. Goerke, B. & Stulke, J. Carbon catabolite repression in bacteria: many ways to make the most out of nutrients. *Nature Rev. Microbiol.* **6,** 613–624 (2008).
25. Shen-Orr, S. S., Milo, R., Mangan, S. & Alon, U. Network motifs in the transcriptional regulation network of *Escherichia coli*. *Nature Genet.* **31,** 64–68 (2002).
26. Walsh, K. & Koshland, D. E., Jr. Characterization of rate-controlling steps *in vivo* by use of an adjustable expression vector. *Proc. Natl Acad. Sci. USA* **82,** 3577–3581 (1985).
27. Wagner, A. *et al.* Computational evaluation of cellular metabolic costs successfully predicts genes whose expression is deleterious. *Proc. Natl Acad. Sci. USA* **110,** 19166–19171 (2013).
28. Oh, M. K., Rohlin, L., Kao, K. C. & Liao, J. C. Global expression profiling of acetate-grown *Escherichia coli*. *J. Biol. Chem.* **277,** 13175–13183 (2002).
29. Balazsi, G., van Oudenaarden, A. & Collins, J. J. Cellular decision making and biological noise: from microbes to mammals. *Cell* **144,** 910–925 (2011).
30. Wang, Z. & Zhang, J. Impact of gene expression noise on organismal fitness and the efficacy of natural selection. *Proc. Natl Acad. Sci. USA* **108,** E67–E76 (2011).


**Supplementary Information** is available in the online version of the paper.

**Acknowledgements** Work in the laboratory of S.J.T. is part of the research programme of the Foundation for Fundamental Research on Matter (FOM), which is part of the Netherlands Organisation for Scientific Research (NWO). D.J.K. was partly supported by an ETH Zurich Postdoctoral Fellowship. We thank T. Shimizu, J. van Zon, H. Bakker, K. Kuipers, M. Ackermann, P.-R. ten Wolde, M. Heinemann and members of the Tans group for reading the manuscript.

**Author Contributions** D.J.K. and S.J.T. conceived and designed the experimental approach. D.J.K., P.N., N.W., V.S. and S.B. performed the experiments. P.N. developed the theoretical model. D.J.K., P.N. and S.J.T. wrote the manuscript.

**Author Information** Reprints and permissions information is available at www.nature.com/reprints. The authors declare no competing financial interests. Readers are welcome to comment on the online version of the paper. Correspondence and requests for materials should be addressed to S.J.T. (tans@amolf.nl) or D.J.K. (kiviet@env.ethz.ch).

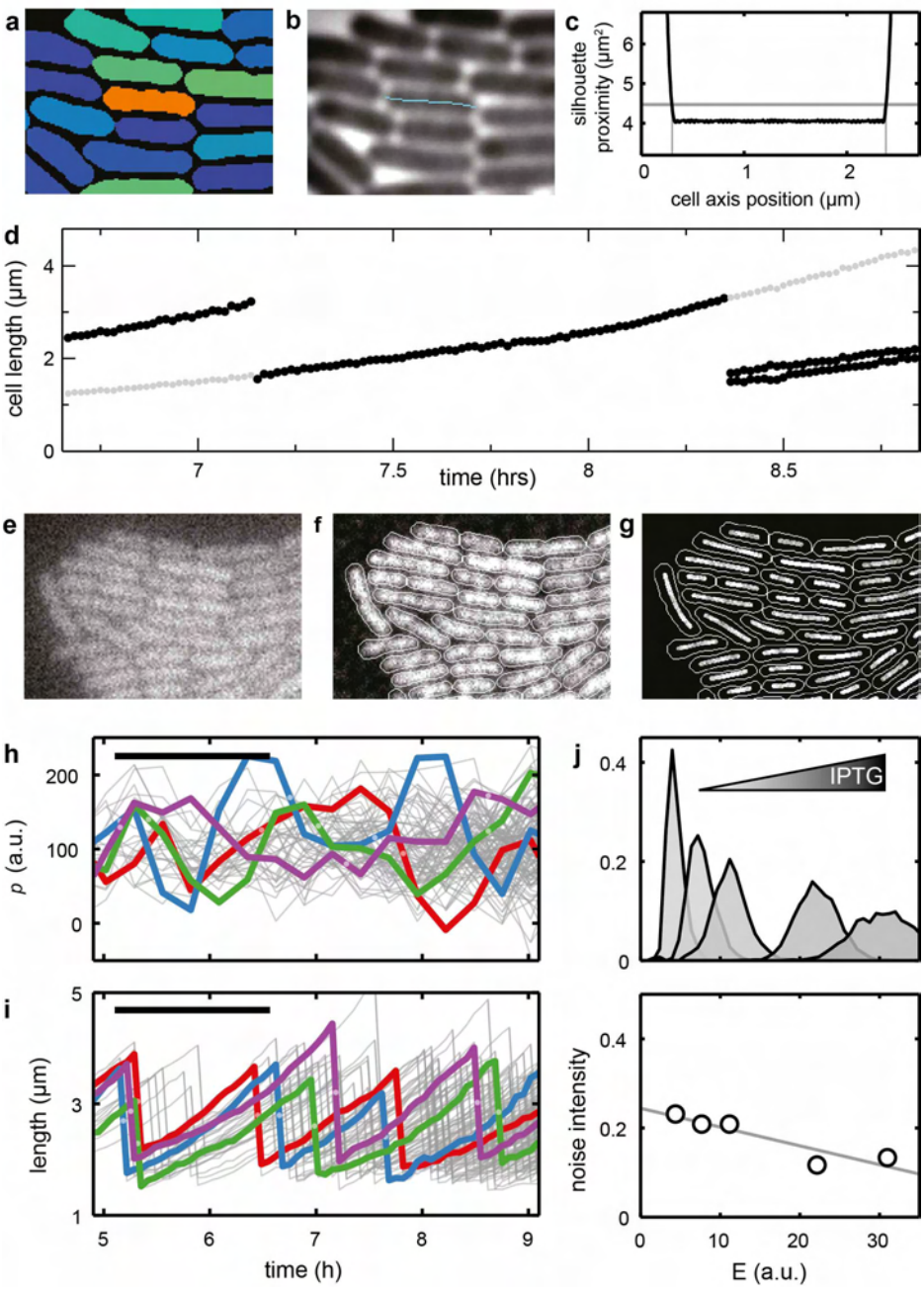


**Extended Data Figure 1 | Image analysis and determination of cell length, elongation rate, enzyme concentration and production rate.** **a**, Segmented cell silhouettes are obtained by applying a Laplacian of Gaussian filter on phase contrast images. **b**, The cell axis is determined by fitting a third degree line through the silhouette. **c**, Cell-length determination. We compute the distances between points on the cell axis and the closest 25 segmentation pixels. The sum of these distances squared, here termed the silhouette proximity, is plotted for points along the cell axis. In the centre of the cell silhouette or mask, the silhouette proximity consistently remains at 4.06 $\mu m^2$, but near the cell poles it rapidly increases. The location of each cell pole was taken at a silhouette-proximity of 4.47 $\mu m^2$. **d**, Elongation rate of a single cell. The length of a single cell, its parent and its offspring plotted over time (dark circles). Instantaneous exponential elongation rate is determined by fitting an exponential to this data for a fraction of the cell cycle. At the beginning and end of each cell cycle, length data of the parent or the offspring are used for this fitting process (grey circles, see Supplementary Information). **e**, Initial fluorescence image. **f**, Image after background correction, shading correction and deconvolution by a point spread function. Total cell fluorescence is determined as the sum of fluorescence values within the cell silhouette. **g**, To determine the cellular fluorescence intensity that reports for the enzyme concentration accurately, we averaged the fluorescence values of pixels within a box of fixed width and equidistant length from the poles inside the cell perimeter. **h**, Enzyme production rate against time $p(t)$ for all lineages within a microcolony, from 5 h into the experiment and onwards. Four lineages are coloured for clarity. Black bar, mean division time; light points, division events. **i**, Cell length against time $L(t)$ as in **h**. **j**, Histograms of observed $E$ values for different IPTG induction levels. Bottom panel indicates the noise intensity, defined as the standard deviation over the mean.

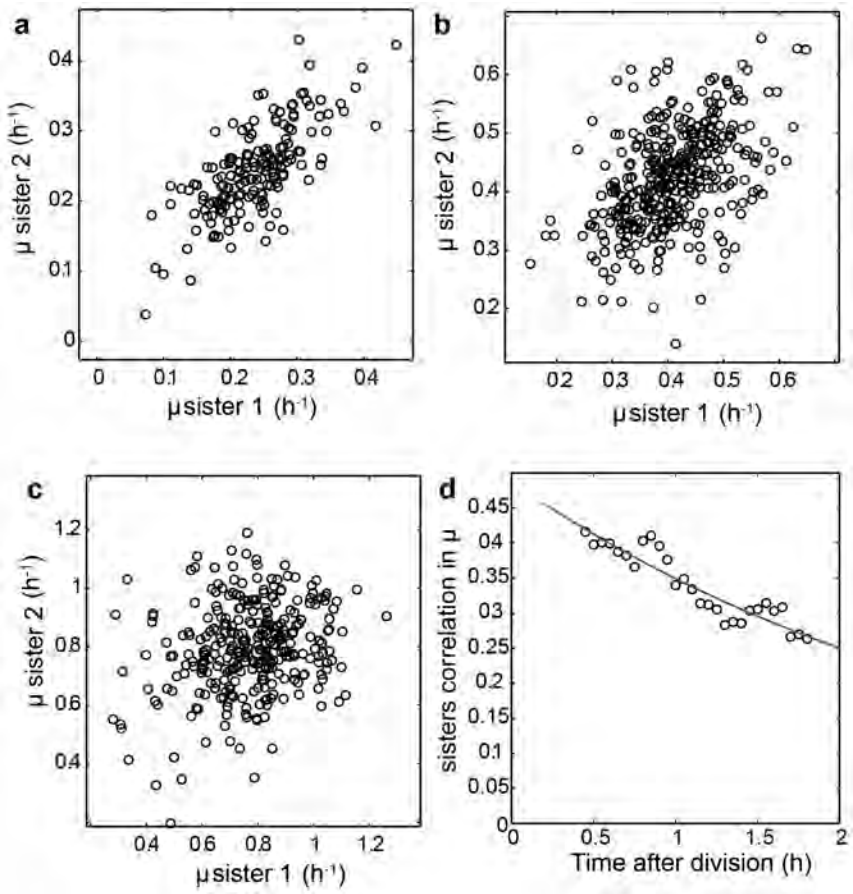


**Extended Data Figure 2 | Correlations between the growth rate of sister cells during growth on lactulose for increasing levels of IPTG induction.** **a**, At 4 μM IPTG, $R = 0.72$, $n = 171$, $P < 10^{-27}$ (*t*-test). **b**, At 6 μM IPTG, $R = 0.42$, $n = 382$, $P < 10^{-16}$. **c**, At 200 μM IPTG, $R = 0.32$, $n = 314$, $P < 10^{-8}$. **d**, Evolution in time of the correlation coefficient between growth rate of sisters, for 6 μM IPTG. A decreasing exponential was fitted with a decay time of 2.86 h.

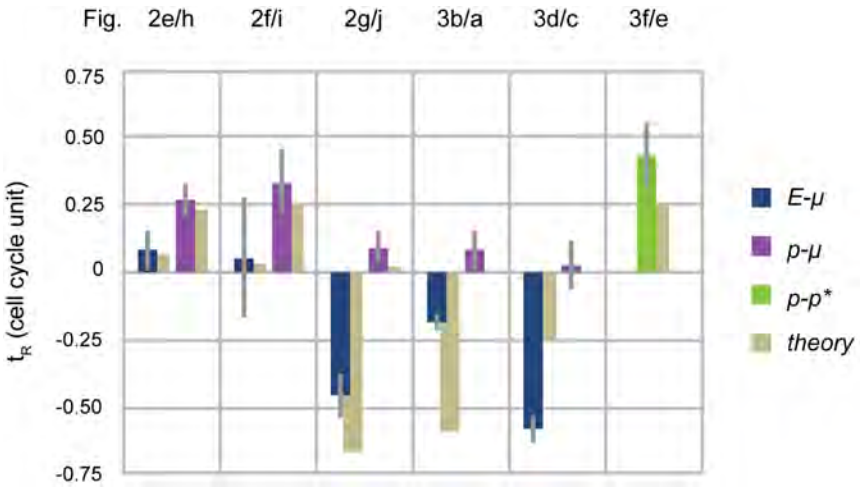


**Extended Data Figure 3 | Quantification of symmetry of cross-correlation functions.** For each cross-correlation (corresponding figure indicated at top), we computed the weighted average of the time delay $\tau_R = \sum_{t=I}(R_t \cdot t) / \sum_{t=I} R_t$, with $R_t$ the correlation intensity at time delay $t$, considering significantly cross-correlations ($t$-test, $P < 0.05$, $n = 4$) within the interval $I = [-2, 2]$ cell cycles. A positive (respectively negative) $\tau_R$ indicates that the cross-correlation $R$ has more weight at positive (respectively negative) times. Error bars denote the standard deviation of the symmetry values determined for four sub-branches. Note that the $E$–$\mu$ cross-correlations of Fig. 3c–d are negative, and hence we display $-\tau_R$.

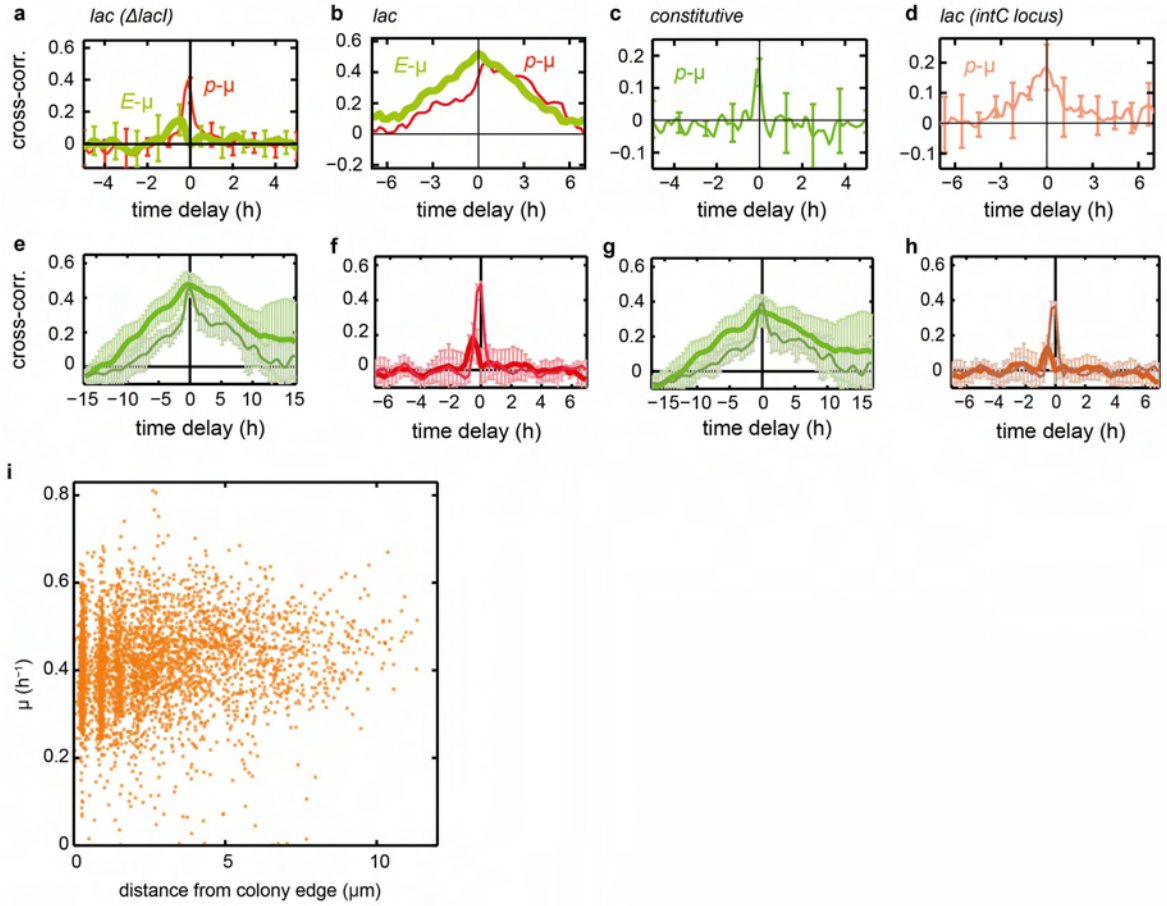


**Extended Data Figure 4 | Cross-correlations of control experiments and using different methods of growth-rate determination.** **a**, Expression of *lac* in a *lacI* repressor knockout strain on lactose minimal medium (to be compared with Fig. 2g). **b**, Expression of *lac* measured with a GFP fusion to LacZ shows same result as co-transcriptional expression of GFP on 0.1% lactulose and 6 μM of IPTG (to be compared with Fig. 2f). **c**, Exogenous constitutive promoter (PN25) driving the production of GFP, inserted in the *cheZ* locus, on minimal medium with lactose. **d**, The *lac* promoter driving the production of yellow fluorescent protein (YFP), inserted in the *intC* locus, on minimal medium with maltose. **e**, Cross-correlations for lactulose growth at low IPTG (4 μM), with growth rate determined as follows: $S(t)$ is the surface area of the cell silhouette versus time (Extended Data Fig. 1a). The growth rate is the time derivative of $S(t)$. **f**, The same, for lactulose growth at high IPTG (200 μM). **g**, Cross-correlations for lactulose growth at low IPTG (4 μM), with growth rate determined as follows: $S(t)$ is the surface area of the cell silhouette versus time, $L(t)$ is the length of the cell silhouette versus time (Extended Data Fig. 1b, c). The growth rate is the derivative of $L(t) \times [S(t)/L(t)]^2$. Note that $S(t)/L(t)$ is taken as a measure for the width of the cell, and the width squared times the length as a measure for the cell volume. **h**, The same, for lactulose growth at high IPTG (200 μM). These cross-correlations display the same shape and symmetry as in Fig. 2e, g, where the growth rate is determined as the derivative of the length of the cell silhouette (Extended Data Fig. 1d). Hence the central features are robust to different methods of growth rate determination. **i**, Scatter plot of instantaneous growth rate and cell position within the microcolony. The cell position was calculated as the minimal distance of the centre of a cell to the edge of the microcolony. Data obtained during growth on lactulose at intermediate IPTG induction (6 μM).

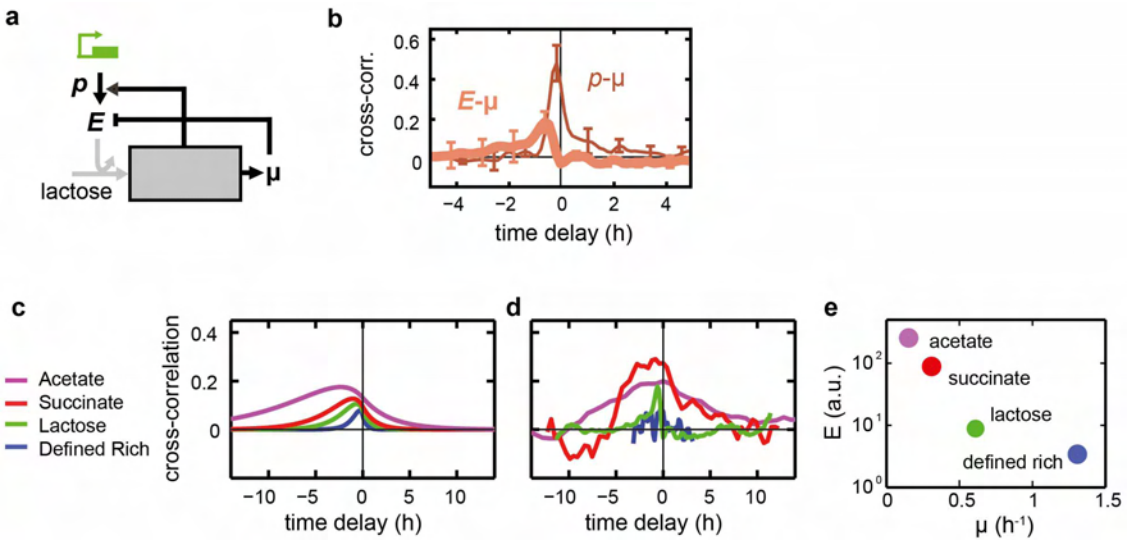


**Extended Data Figure 5 | Cross-correlations for growth on different carbon sources.** **a**, Schematic diagram of noise transmission during growth on lactose, which is predicted to be similar to the case of growth on lactulose at high IPTG induction (see Fig. 2g, j). **b**, Corresponding measured cross-correlations. **c**, Theoretical cross-correlations obtained by using the parameters during growth on lactulose and changing exclusively the population average growth rate to the experimentally measured value. This prediction displays a positive asymmetric peak towards negative time and a width scaling with the average growth rate. **d**, Corresponding measured cross-correlations. **e**, Population average *lac* enzyme concentration versus the population average growth rate on minimal medium supplemented with varying carbon sources.

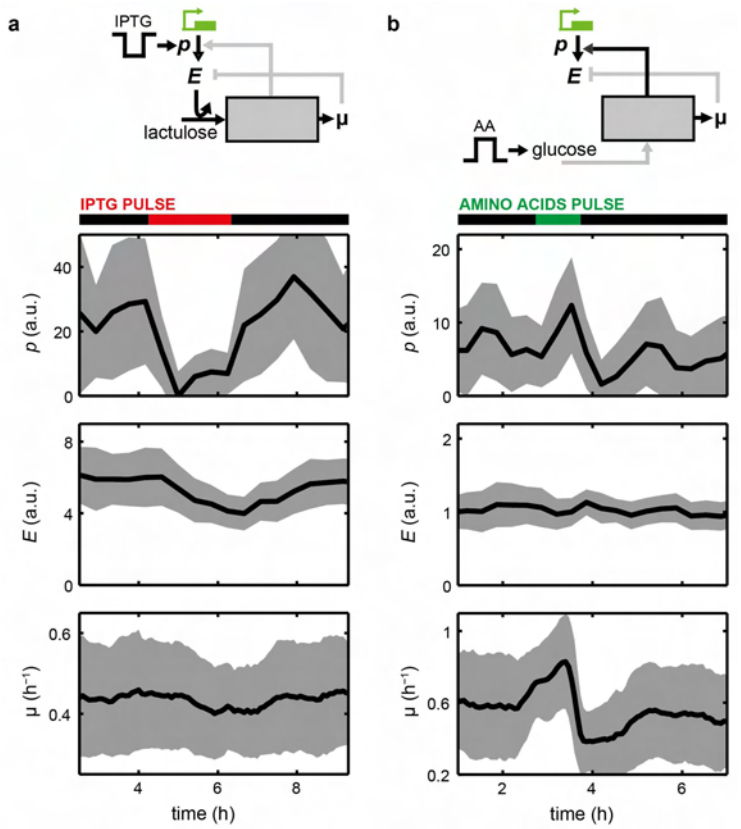


**Extended Data Figure 6 | External media perturbations in microfluidic device.** **a**, Growth of AB460 in microfluidic device (see Supplementary Information) on M9 medium with 0.1% lactulose, 0.01% Tween-20 and 16 μM IPTG. A 2-h pulse to medium with 3 μM IPTG is indicated in red. Black line is the mean, and grey area is the standard deviation, of approximately 60 cells. Indicated are the lac production rate ($p$), lac concentration ($E$) and cell growth rate ($\mu$). The duration and intensity of the pulse was chosen to reflect the naturally occurring fluctuations in *lac* expression. Upon the pulse, the production rate transiently decreased, followed by a gradual transient decrease in *lac* concentration, and a transient decrease in growth rate. These data are consistent with the catabolism transmission mode (top). **b**, Growth of ASC631 in microfluidic device on M9 medium with 0.1% glucose, 0.01% Tween-20 and 1 mM IPTG. To mimic fluctuations in common components, a 1-h pulse of amino acids (Teknova M2104) added to the medium is indicated in green. Both growth and production rate increase immediately upon addition of amino acids, reflecting the common noise transmission mode (top). The enzyme concentration remained relatively stable, showing that for these perturbations the production increase and dilution increase cancelled each other. These data are consistent with the common noise mode (top).

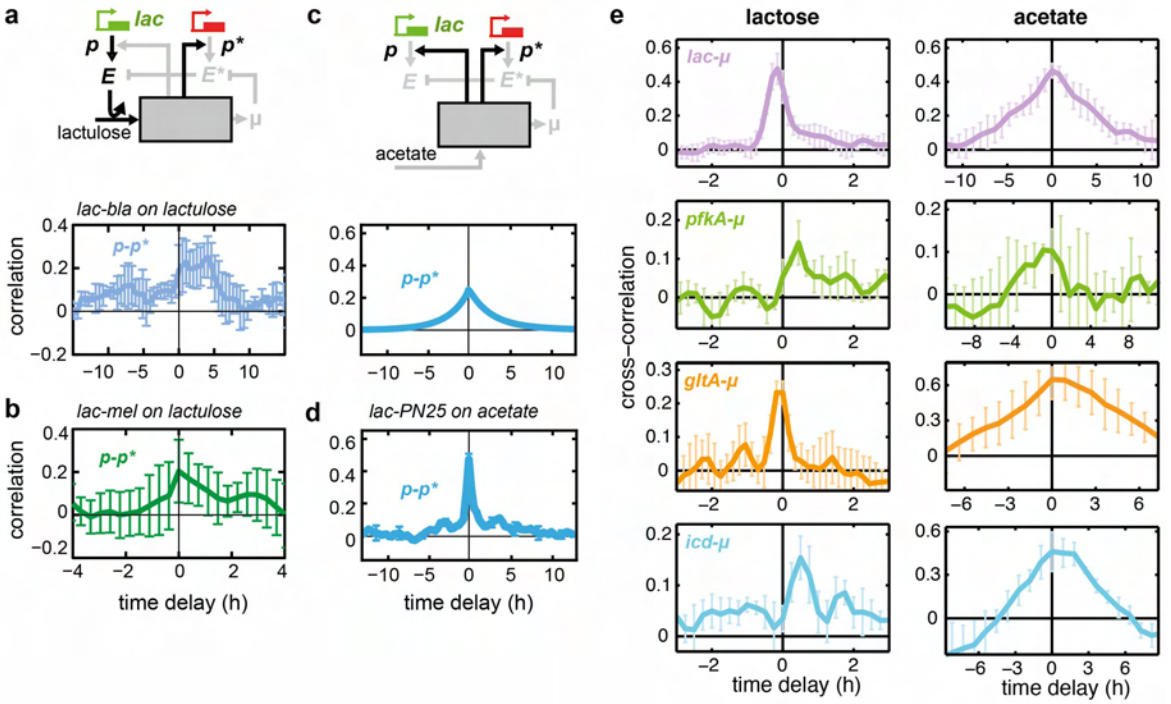


**Extended Data Figure 7 | Cross-correlations of additional constructs.** **a**, Transmission from *lac* to another gene via growth (on 0.1% lactulose and 6 μM IPTG) shown by the asymmetric cross-correlations between *lac* production rate and mCherry production driven by the constitutive *bla* promoter. **b**, The same for *lac* production rate and mCherry driven by the *mel* promoter induced by 0.2% melibiose (*ΔmelA* strain). **c**, Symmetric cross-correlation between *lac* production rate *p* and other gene production rate *p** predicted for growth on acetate (see **d**). **d**, Absence of transmission shown by the cross-correlation between *lac* production rate *p* and the mCherry production rate *p** driven by the constitutive PN25 promoter, on minimal medium with 0.1% acetate, consistent with predictions (**c**). **e**, Cross-correlations ($R_{p\mu}$) for *lac*, *pfkA*, *gltA* and *icd* in lactose (left) and acetate media (right).

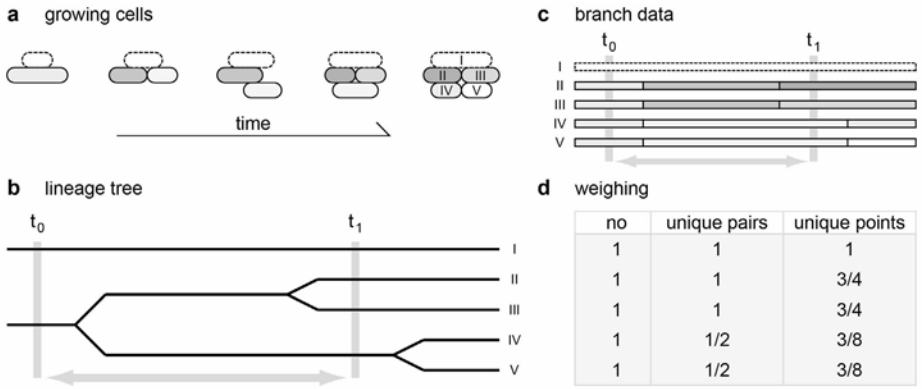


d weighing

| no | unique pairs | unique points |
|---|---|---|
| 1 | 1 | 1 |
| 1 | 1 | 3/4 |
| 1 | 1 | 3/4 |
| 1 | 1/2 | 3/8 |
| 1 | 1/2 | 3/8 |

**Extended Data Figure 8 | Extracting and weighing lineages from a branched data set.** **a**, Depiction of a growing microcolony over time, starting with two cells on the left and growing into five cells on the right. **b**, A lineage tree of the data shown in **a**. The tree starts with two lines (left), indicating the two starting cells, and at each division the line splits, resulting in five cells at the end (right). **c**, Five lineages can be extracted from the data. Note that most lineages share part of their data. When correlating data points from $t_0$ with $t_1$, one pair consists of completely independent data points (lineage I). Two lineages provide exactly the same pairs of data points (lineages IV and V), and two lineages only share a data point at $t_0$ (lineages II and III). **d**, Different types of weighing for the correlation of data points from $t_0$ with $t_1$ as used in equation (6) in Supplementary Information. No: each lineage is weighed equally. Unique pairs: weighing such that only comparisons between unique data pairs are used. Unique points: lineages II and III are not completely independent, which can be corrected for by this weighing from equation (5) in Supplementary Information.

**Extended Data Table 1 | Contribution of noise transmitted from *lac* concentration *E* to different variables in various culture media**

| Lactulose experiments | Noise observed in | Transmitted from E |
|---|---|---|
| low induction | p | 12% |
| (iptg = 4 μM) | E | 34% |
| | μ | 31% |
| intermediate induction | p | 9.80% |
| (iptg = 6 μM) | E | 19% |
| | μ | 20% |
| Constitutive gene | p* | 13% |
| (iptg = 6 μM) | E* | <1% |

The contribution of noise transmitted from *E* was computed by comparing the coefficient of variation of a given variable with or without transmission from *E*, using the values fitted with the model. Note that a decomposition of noise as a sum of coefficient of variations is not possible here, given the feedback of *E* on itself, which leads to self-sustained fluctuations which impact the noise intensity in a non-additive way.

**Extended Data Table 2 | List of strains used in this study**

| Strain | Genotype | Origin |
|---|---|---|
| AB460 | *ΔlacA::gfp-cat* | Constructed by A. Böhm |
| ASC631 | *ΔlacA::gfp-cat, Δphp::$P_{N25}$-mCherry-kan$^R$* | This study |
| ASC636 | *ΔlacA::gfp-cat, ΔCheZ::$P_{N25}$-mCherry-kan$^R$* | This study |
| ASC638 | *ΔCheZ::$P_{N25}$-gfp-kan$^R$* | This study |
| ASC639 | *ΔlacA::gfp-cat, ΔlacI::kan$^R$* | This study |
| ASC662 | *lacZ-gfp* | This study |
| ASC640 | *ΔlacA::gfp-cat, Δphp::Bla-mCherry-kan$^R$* | This study |
| ASC644 | *ΔlacA::gfp-cat, ΔmelA::mCherry-kan$^R$* | This study |
| ASC666 | *L31::mChery- kan$^R$, gltA::gfpA206K-cat* | This study |
| ASC677 | *L31::mCherry-kan$^R$, pfkA::gfpA206K-cat* | This study |
| ASC678 | *L31::mCherry-kan$^R$, icd::gfpA206K-cat* | This study |
| MG22 | *ΔintC PL –lac01::yfp* | Elowitz lab |
| NCM520 | *ΔlacAYZ* | Obtained from the Coli Genetic Stock Center |